Energy Proceedings
Vol 55, 2025
ISSN 2004-2965

A preliminary study of C@Fe_3O_4 for gas separation of CH_4 and CO_2[#]

Longlong Lei[1,2] Hang Yuan[1,2] Hongguang Zhu[1,2,*] Fanghui Pan[1,2] Fulu Lu[1,2]
1. School of Mechanical Engineering, Tongji University, Shanghai 201804, China
2. Bio-Energy Research Center, Institute of New Rural Development, Tongji University, Shanghai, 201804, China
(Corresponding author: E-mail address: zhuhg@tongji.edu.cn)

ABSTRACT

Biogas, produced through the anaerobic digestion (AD) process of biomass, is one of the most promising renewable energy sources. Besides CH_4, biogas contains other components that negatively impact its direct application, such as H_2S, CO_2, NH_3, and siloxanes. Among these, CO_2 has the most significant effect on reducing the calorific value of biogas, with its content reaching 30%-45%. Therefore, the separation of CO_2 from biogas using solid adsorbents for biogas upgrading has been a widely studied topic in recent years. Previous theoretical studies have found strong interactions between Fe_3O_4 and CO_2, indicating a high CO_2-specific adsorption capacity. However, the low specific surface area of Fe_3O_4 limits its CO_2 loading capacity. Coating the surface of Fe_3O_4 with a carbon layer to form carbon-coated magnetite (C@Fe_3O_4) can significantly increase its specific surface area, making Fe_3O_4 a promising new CO_2 adsorption material. In this study, a novel C@Fe_3O_4 material was prepared using concentrated organic matter from biogas effluents and iron oxide through a hydrothermal-carbonization process. This material achieved a specific surface area of up to 187.50 m^2/g. Under conditions of 1 bar and 37°C, the material demonstrated a selectivity for CO_2 over CH_4 of up to 10.5, outperforming most adsorbent materials. Its CO2 adsorption capacity was measured at 0.56 mmol/g (0.99 $mmol/cm^3$).This material supports the development of a new, efficient, low-energy, and low-cost pressure swing adsorption (PSA) process for CO_2 and CH_4 purification.

Keywords: C@Fe_3O_4, gas separation, CO_2 adsorption, biogas purification

NONMENCLATURE

Abbreviations	
AD	anaerobic digestion
PSA	pressure swing adsorption
Symbols	
n	Year

1. INTRODUCTION

With the development and growth of the world economy, the demand for energy in many countries has increased sharply. Currently, over 85% of the energy required for daily production activities still comes from fossil fuels[1]. The combustion of fossil fuels produces carbon dioxide (CO_2), which has significantly altered the composition of the Earth's atmosphere. Over the past 15 years, global warming has become a major issue in global environmental studies. The cause of global warming is the substantial increase in greenhouse gases such as CO2, CH4, N2O, HFCs, PFCs, and SF6, with CO_2 emissions being the primary contributor. This represents the largest environmental problem worldwide today. Given this situation, the research and development of clean energy have become critical areas of modern energy studies. Methane fuel (biogas) is an important clean energy source. The CO_2 emissions from biogas production are significantly lower than those from fossil fuels, leading to increasing demand for biogas. Biogas typically contains 40-75% methane (CH_4), 25-60% CO_2, and small amounts of other components, such as H_2O and H_2S. Upgrading biogas by absorbing and separating CO_2 from CH_4 can increase the purity of CH_4, making it a high-quality fuel and enabling its use in the production of chemical products[2].

The presence of CO_2 in biogas not only reduces its calorific value but also causes pipeline corrosion during transport. Therefore, separating CO_2 from biogas has become a topic of great interest among scholars in this field. In industrial practice, water scrubbing, PSA, chemical scrubbing, and membrane separation are the technologies currently applied in biogas upgrading[3]. However, water scrubbing, chemical scrubbing, and membrane separation each have their drawbacks: high energy consumption, ammonia loss, and high costs, respectively. PSA technology is often recommended for biogas purification due to its low cost, simple operation, and flexibility, which suits the typical variable supply and demand of biogas facilities[4,5]. The efficiency of PSA largely depends on the choice of adsorbent, which

[#] This is a paper for the 16th international Conference on Applied Energy (ICAE2024) Sep. 1-5, 2024, Niigata, Japan.

should exhibit good selectivity for CO_2 over CH_4. Additionally, the adsorbent should possess thermal stability, chemical inertness, and a high specific surface area[6].

Previous studies have shown that zeolite adsorbents, porous activated carbon, and metal-organic framework materials have significant potential for selective CO_2 adsorption. Activated carbon, in particular, is considered a promising adsorbent for industrial applications due to its economical synthesis from waste biomass materials and simple production methods. However, activated carbon generally lacks selectivity for gas adsorption and requires modifications to achieve selective CO_2 adsorption. Atomic doping can effectively enhance the CO_2 selectivity of activated carbon. Ning et al. [7] prepared N-doped activated carbon through direct annealing and found a significant improvement in CO_2 selectivity. Xiao et al. [8] demonstrated that, besides N-doping, S-doping also enhances the CO_2 adsorption capacity of activated carbon. Moreover, several studies have shown that doping oxygen-containing functional groups on the surface of activated carbon can improve CO_2 adsorption properties and selectivity [9,10,11].

Increasing the specific surface area and optimizing the pore structure of activated carbon is another effective method to enhance adsorption capacity [12,13]. Chemical activation of carbon precursors derived from biomass residues is a common approach to improve pore structure and specific surface area [14-16]. Chemical activation, a one-step technique, involves impregnating the raw sample or mixing it with chemical agents. Various chemical activating agents, including KOH, NaOH, K_2CO_3, H_3PO_4, H_2SO_4, HCl, $MgCl_2$, MgO, $AlCl_3$, and $ZnCl_2$, have been studied [17-25]. These agents facilitate proper dehydration, cross-linking, and the formation of a rigid matrix [19]. This method avoids calcination, thereby preventing volatile losses and volume shrinkage, resulting in a higher yield of activated carbon [26]. Additionally, fundamental physical studies have revealed a unique CO_2 adsorption mechanism on Fe_3O_4. Theoretical calculations [27] indicate strong interactions between CO_2 and the Fe_3O_4{001} and {111} surfaces. Initially, CO_2 adsorbs on the Fe^{2+}-related defects on Fe_3O_4{001}, forming a physically adsorbed monolayer. The interaction with the surface causes the CO_2 molecule to bend, creating a highly stable carbonate-like group, where the C atom is atop the surface O, and the O atoms in the molecule point toward the coordinated Fe^{3+} ions. This multilayer adsorption mechanism has been confirmed in previous studies [27-28], with the C-O bond length in the molecule increasing by 0.09 Å compared to the free molecule. On the Fe_3O_4{111} surface, CO_2 adsorption occurs in two modes: strong and weak adsorption [29]. The weak interaction is facilitated by van der Waals forces between the Fetet1 site on the surface and the CO_2 molecule. The strong interaction involves horizontal configuration adsorption of CO_2 at the $Fe_{oct2\text{-}tet1}$ site, where electrons transfer from Fe_3O_4 to the C atom in CO_2, forming a C-O bond with the O atoms on the Fe_3O_4{111} surface. Therefore, coating a carbon structure on the surface of Fe_3O_4 is expected to combine the high specific surface area of porous carbon with the unique CO_2 adsorption properties of Fe_3O_4, resulting in a novel adsorbent.

In this study, a novel C@Fe_3O_4 material was synthesized using iron oxide and biogas effluent as raw materials. The raw materials underwent a hydrothermal-calcination method combined with KOH impregnation and etching, resulting in a carbon-coated magnetite nanomaterial with a high specific surface area. The prepared material was characterized, and its adsorption properties for CO_2 and CH_4 were analyzed. The results showed that the synthesized material exhibited good selectivity for CO_2 over CH_4. This research provides a stable, cost-effective, and recyclable method for preparing high specific surface area magnetic nano C@Fe_3O_4. For the first time, C@Fe_3O_4 was applied as a separation adsorbent for CO_2 and CH_4. Additionally, the study utilized Aspen Adsorption software to simulate the application of this adsorbent in PSA processes. The simulation results further confirmed that this material is an excellent industrial adsorbent for methane purification via PSA. This material lays a high-selectivity foundation for separating CO_2 from methane in the biogas industry.

2. MATERIAL AND METHODS

2.1. Material

The carbon source used in this experiment was biogas effluent, obtained from a biogas plant in Funan County, Fuyang City, Anhui Province, China. The iron oxide used in the study was purchased from China Metallurgical Group Corporation, with an average particle size of 1 micron. The KOH solution used in the impregnation stage was a 1 mol/L standard solution, purchased from Sinopharm Group.

2.2. Material Preparation

The sample preparation process is illustrated in Figure 1. First, 2 grams of iron oxide were placed into 20 mL of concentrated anaerobic digestion liquid. The

mixture was stirred for 12 hours using a magnetic stirrer and then transferred into a high-temperature high-pressure autoclave for a hydrothermal reaction at 200°C for 12 hours. After natural cooling to room temperature, the mixture was transferred to a tubular rotary furnace. In an oxygen-free environment, the anaerobic digestion liquid and iron oxide mixture slowly transformed into carbon-coated magnetic nano-ferrite (C@Fe_3O_4). During calcination, the temperature was increased at a rate of 600°C/h. Once the temperature reached 600°C, it was maintained for 2 hours. During the first 1.5 h, nitrogen gas was introduced into the rotary furnace at a flow rate of 2 L/min to create an oxygen-free environment and carry away water vapor. In the subsequent 1.5 h, the nitrogen gas flow rate was reduced to 20 mL/min, ensuring a positive pressure environment in the furnace as the water content had already been completely removed. After carbonization and cooling to room temperature, the sample was crushed using a spatula and washed three times with anhydrous ethanol and deionized water, respectively. Finally, the sample was dried at 60°C, resulting in the final product, MNCFT. Additionally, to verify the necessity of the calcination process, a new set of experiments was conducted with the same raw materials, but without the calcination step. The sample obtained from this set was named ICG.

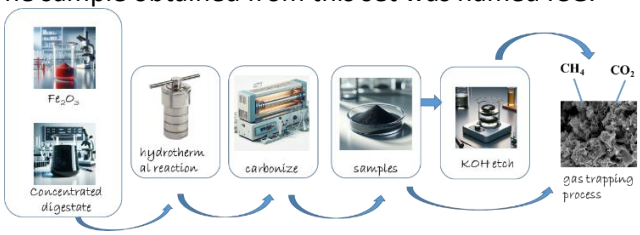

Fig. 1.Schematic diagram of the preparation of carbon-based ferric tetraoxide

After confirming that MNCFT is magnetic carbon-coated nano-ferrite, it was impregnated and activated using a 1 mol/L KOH solution. The specific steps are as follows: 2 grams of MNCFT were placed into 100 mL of KOH solution. The mixture was then stirred at room temperature for 48 hours using a mechanical stirrer. After stirring, the sample was washed five times with deionized water. The wet solid was then dried at 60°C. The resulting product was named UMNCFT.

2.3. Characterization method

The SEM tests were conducted using a Zeiss Sigma 300 scanning electron microscope to observe the microscopic morphology. The acceleration voltage was set between 0.02-30 kV. For higher stability, the probe current ranged from 3 nA to 20 nA, and the SE2 secondary electron detector was employed. XPS tests were performed using a Thermo Scientific K-Alpha X-ray photoelectron spectrometer to determine the elemental composition and content on the sample surface. The excitation source was Al Kα radiation (hv=1486.6 eV) with a spot size of 400 μm. The pass energy for the full spectrum scan was 100 eV with a step size of 1 eV, and for the narrow spectrum scan, the pass energy was 50 eV with a step size of 0.1 eV. At least five cycles of signal accumulation were conducted. XRD tests were carried out using an X'Pert PRO MPD X-ray diffractometer to determine the crystallinity and composition of the samples. The target material was copper, with a scanning range of 10-80 degrees and a scanning speed of 2°/min. TEM tests were performed using a FEI Tecnai F20 transmission electron microscope to observe the microstructure and crystal morphology of the samples. Micro-grid copper nets were used for sample preparation. BET tests were conducted using a JWBK200B fully automatic specific surface area and porosity analyzer. All samples were degassed at 200°C for 3 hours to remove volatiles before characterization. The N2 adsorption isotherms were obtained at 195 K and partial pressure range (0.005-0.99). The BET surface area, pore volume, and pore size distribution were estimated using non-local density functional theory (NLDFT). FTIR tests were performed using a Shimadzu IRAffinity-1S Fourier transform infrared spectrometer to analyze the functional groups and composition of the samples. The wavenumber range was 400-4000 cm-1, and the number of scans was 32.

2.4. Gas adsorption and separation characterization

Samples were tested for static CO_2 and CH_4 adsorption at different temperatures using a Micromeritics ASAP2460 instrument. Before conducting the adsorption tests, the samples were degassed at 300°C for 2 h. Then, the gas pressure was increased to 1 bar to collect the isotherms. The adsorption equilibrium data for CO_2 and CH_4 at different temperatures were modeled using the BET isotherm model. The form of this isotherm model is shown below:

$$\frac{V^{\alpha}}{V_m^{\alpha}} = \frac{c(p/p^*)}{\left(1-\frac{p}{p^*}\right)[1+(c-1)p/p^*]}$$

In the equation, V^{α} is the adsorption amount at pressure p, V_m^{α} is the saturation adsorption amount of a monolayer, p^* is the saturation vapor pressure of the adsorbate liquid at the adsorption temperature, and c is the adsorption constant related to the heat of adsorption. After obtaining the isothermal adsorption lines for CO_2 and CH4 at 25°C, the IAST calculations were performed using the ChromWorks software package.

The separation characteristics of CH_4 and CO_2 were tested using a multi-component selective competitive adsorption analyzer, model BSD-MAB, manufactured by Beijing Beishide. Before the test, the sample was degassed at 300°C for 3 h to activate the sample by heating under vacuum conditions. The separation characteristics of the sample for CH_4 and CO_2 were then studied under conditions of 25°C and 1 bar. Aspen Adsorption was used to simulate the CH_4/CO_2 breakthrough curves at different pressures and pressure differentials.

3. RESULTS

3.1. Material Characterization Results

To investigate the phase composition of MNCFT, UMNCFT, and ICG, XRD tests were conducted on all three samples. The results are shown in Figure 2a. The characteristic peaks of MNCFT and UMNCFT align closely with those of Fe3O4. This indicates that the main crystalline phase of both samples is Fe3O4. The reason for this is that the digestate contains a large amount of humic acid, which has numerous carboxyl, phenolic hydroxyl, and carbonyl groups that have a strong complexing ability with iron oxide. Moreover, the waste digestate possesses strong reducing properties, providing many electrons to reduce iron oxide to Fe3O4 crystals. The spectrum of ICG is consistent with Fe2O3. This is because the reducing substances in the anaerobic digestate have a high activation barrier and require sufficiently high temperatures to provide electrons for the reduction of Fe. This study shows that a temperature of 600°C is sufficient to activate the reducing substances in the digestate, while 200°C is not high enough. To explore the surface functional groups of the products, UMNCFT was subjected to FTIR analysis. The results are shown in Figure 2b. The results indicate that the product contains abundant organic components. The infrared spectrum shows vibrations of bonds such as O-H, C=O, C=C, C-H, C-O, and C-O-C.

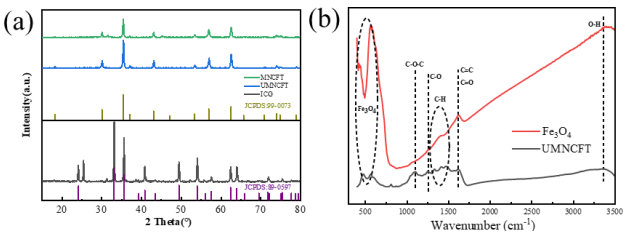

Fig. 2. XRD patterns of different process products (a); Fourier spectrum of UMNCFT (b)

After the hydrothermal process, Fe_2O_3 can fully mix with the anaerobic digestate. Therefore, the SEM images of MNCFT (Figure 3a-b) show uniformly sized and spatially distributed nano-polygonal particles, with a particle size of approximately 300 nm. The TEM images (Figure 3e-f) also support this conclusion. Furthermore, the high-resolution TEM images show distinct lattice fringes, consistent lattice fringe orientation, and clear lattice fringes. Combined with the sharp peaks in its XRD spectrum, this indicates good crystallinity of MNCFT. The TEM images of MNCFT also reveal an obvious core-shell structure, which is further supported by the differences in the XPS and EDS elemental semi-quantitative analysis results.

Table 1.Results of semi-quantitative analysis of XPS and EDS elements of MNCFT

Element	C	O	Fe
XPS Wt%	81.1	16.7	2.2
EDS Wt%	16.66	29.27	54.07

As shown in Table 1, XPS elemental semi-quantitative analysis primarily measures the relative content of elements on the material's surface. The results indicate that the Fe content on the material's surface is only 2.16%, while the C content is 81%. EDS elemental semi-quantitative analysis measures the overall relative elemental content of the material, showing that the Fe content in the material is 23.1%, and the C content is 33.15%. This suggests that the surface of the material is primarily composed of carbon, while the interior is mainly Fe_3O_4. To observe the morphological changes before and after activation, SEM (Figures 3c-d) and TEM (Figures 3g-h) images of UMNCFT were taken. The SEM images of UMNCFT show a more porous surface structure, which is beneficial for gas adsorption and storage.

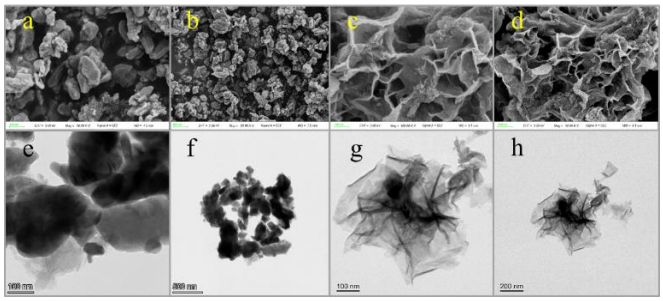

Fig. 3. SEM images of MNCFT (a-b); SEM images of UMNCFT (c-d); TEM images of MNCFT (e-f); TEM images of UMNCFT (g-h)

The N_2 isothermal adsorption curves of MNCFT and UMNCFT at 195 K were measured (Figure 4a). The NLDFT model was used to calculate their pore volume and pore size distribution (Figure 4b). Both UMNCFT and MNCFT have pore sizes between 3-5 nm, indicating a large presence of micropores. Since CO_2 is primarily stored in micropores, this porous structure enhances their CO_2 adsorption capacity. The average pore size of UMNCFT is

3.43 nm, with a pore volume of 0.161 cm^3/g. The average pore size of MNCFT is 3.73 nm, with a pore volume of 0.091 cm^3/g. The pore volume of the activated material increased by 77%. The BET specific surface area of the activated material increased by 92%, from 97.87 m^2/g for MNCFT to 187.50 m^2/g for UMNCFT.

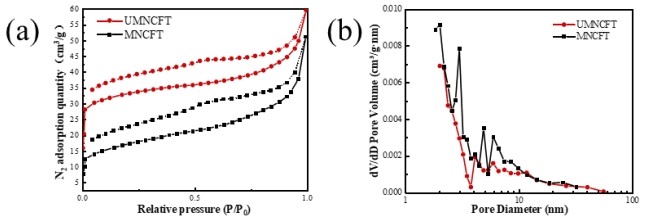

Fig. 4. N_2 adsorption and desorption curves (a) and pore distribution curves (b) for UMNCFT and MNCFT at 195 K

3.2. Gas adsorption properties

The gas adsorption properties of UMNCFT for CO2 and CH4 were a focal point of this study. The isothermal adsorption curves for both gases at 37°C were measured and compared on the same coordinate system (Figure 5a). At 1 bar, UMNCFT exhibited an adsorption capacity of 0.098 mmol/g for CH4 and 0.423 mmol/g for CO2. The adsorption capacity of UMNCFT for CO2 is 4.3 times that for CH4. This substantial difference in adsorption capacity indicates the potential of UMNCFT as a separation adsorbent for CO2 and CH4. Subsequently,

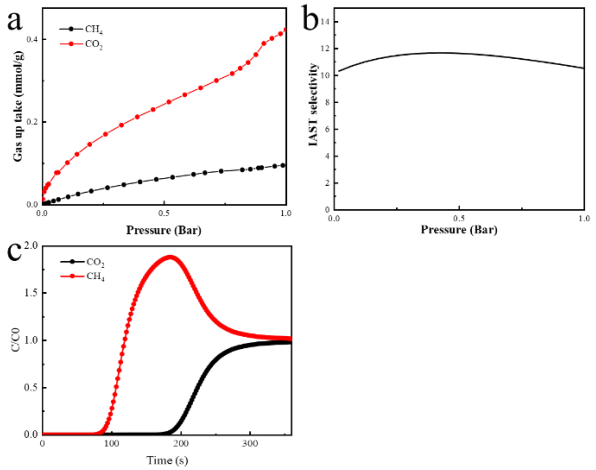

Fig. 5. Isothermal adsorption curves of CH_4 and CO_2 for UMNCFT at 37°C (a); CO_2/CH_4IAST selectivity curve of UMNCFT at 37°C (b); penetration curve of a mixture of CO_2 and CH_4 (50:50) at 25°C

the selectivity of UMNCFT for CO2 and CH4 was calculated using IAST theory. The results (Figure 5b) show that at 37°C and 1 bar, UMNCFT exhibits a high selectivity for CO2 over CH4, with a selectivity factor of 10.5. This is an excellent result. To further investigate the dynamic separation performance of this material for CO2 and CH4, breakthrough curves for a CO2/CH4 (50:50) gas mixture were measured at 1 bar and 25°C (Figure 5c). The results demonstrate that UMNCFT can effectively separate CO2 and CH4. Due to the material's specific adsorption capacity for CO2, no CO2 signal was detected in the first 3 minutes of the experiment. This method can efficiently separate CO2 from biogas, thereby increasing the purity of CH4.

To investigate the effect of pressure and pressure difference between inlet and outlet on the separation of CO_2 and CH_4 gases, Aspen Adsorption software was used to simulate the separation performance under different pressures and pressure differences. The results are shown in Figure 6. Figures 6a-c demonstrate that when the pressure difference between the inlet and outlet is constant, an increase in outlet pressure leads to an earlier appearance of the CO_2 signal at the outlet. This indicates that higher pressure causes the adsorbent to reach saturation for CO_2 adsorption more quickly. Figure 6d shows that when the outlet pressure is constant, an increase in the pressure difference between the inlet and outlet results in an earlier detection of high concentration CH_4 at the outlet. It also causes the adsorbent to reach saturation for CO_2 adsorption more quickly. This impact is more significant compared to the effect of changes in outlet pressure.

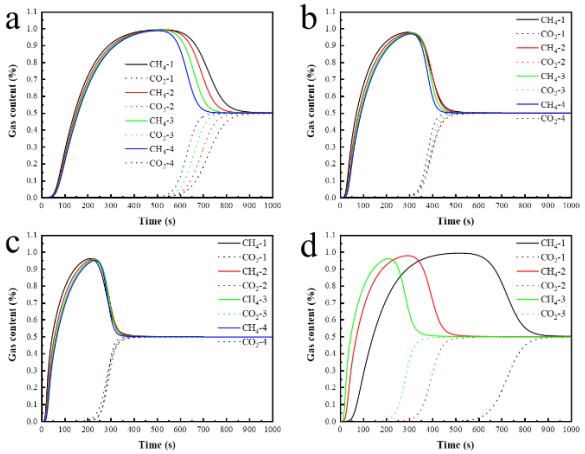

Note: a, b, c are the results of different outlet pressures at 0.1bar, 0.2bar, 0.3bar differential pressure respectively, CH_4-1 represents an outlet pressure of 1bar; d is the result of different inlet/outlet differential pressures at 1bar outlet pressure, CH_4-0.1 represents an inlet/outlet differential pressure of 0.1bar.

Fig. 6. Penetration curves of CO_2 and CH_4 mixed components for different outlet pressures and inlet/outlet differential pressures

The high selectivity of this material for CO_2 is related to its primary phase of Fe_3O_4 crystals. Recent studies have shown that there is a strong interaction between CO_2 and Fe_3O_4. Evidence suggests that this strong interaction does not disappear even when a layer of C structure is coated on the surface of Fe_3O_4. The high

selectivity of UMNCFT for CO_2 is also related to the chemical reactions during its synthesis process. When digestate reacts with Fe_2O_3 at high temperatures, a large amount of CO_2 gas is produced. The evolution of CO_2 gas creates numerous pores in the material that are suitable for CO_2 storage. These pores are precisely suited for CO_2, making it difficult for CH_4 molecules, which have a regular tetrahedral structure, to occupy these pores. Additionally, the high selectivity of the material for CO_2 is partly due to the presence of many oxygen-containing functional groups in the organic layer on the surface of the material. FTIR analysis confirmed that the material has many carboxyl, hydroxyl, and C-O-C functional groups. These functional groups have been shown in other studies to be beneficial for CO_2 adsorption .

4. CONCLUSIONS

In summary, nanocarbon-based Fe3O4 rich in surface functional groups has been synthesized through a hydrothermal-carbonization reaction. The required raw materials for the reaction are inexpensive iron oxide and digestate extract. The CO2 gas released during the reaction creates a rich porous structure and spaces suitable for CO2 storage, resulting in a large specific surface area and high CO2 capture capacity. The magnetic structure of the Fe3O4 core endows the material with strong CO2 adsorption ability. The outer organic coating structure supports the porous structure and further enhances the CO2 adsorption capacity with its surface rich in functional groups. The abundant oxygen-containing functional groups on the surface also favor CO2 adsorption while being unfavorable for H2 adsorption. These two aspects contribute to the extremely high selectivity of the material for CO2. Gas breakthrough tests and simulation results for CO2 and CH4 mixtures indicate that this material can directly produce high-purity CH4 in a single adsorption stage. These characteristics make the material a highly promising adsorbent for biogas purification.

ACKNOWLEDGEMENT

We gratefully acknowledge the support of the Special Project of International Exchange Program for Graduate Students, Tongji University, Municipal-school Cooperation in Science and Technology (Grant nos. SXHZ202206) and Shanghai “Super Postdoc” incentive program [Grant nos. 2023789]. This work supported by Shanghai Linhai Ecological Technology Co., LTD and Funan Linhai Ecological Technology Co., LTD. We would like to thank Mr. Yinli-Zhang, Hongfeng-Hu, Jianlin-Zhao and Xin-Zhang from Shanghai Linhai Ecological Technology Corp., Mr. Xiang-Li from Funan Linhai Ecological Technology Co., LTD for in situ sample collection.

REFERENCE

[1] K. Zhou, S. Chaemchuen, F. Verpoort, Alternative materials in technologies for Biogas upgrading via CO_2 capture. Renwable and Sustainable Energy Reviews. 2017,79:1414-1441.

[2] Y. Jiang, J. Ling, P. Xiao, Y. He, Q. Zhao, Z. Chu, Y. Liu, Z, Li, P.A. Webley, Simultaneous biogas purification and CO_2 capture by vacuum swing adsorption using zeolite NaUSY. Chem. Eng. J. 2018,334:2593-2602.

[3] E. Ryckebosch, M. Drouillon, et al. Techniques for transformation of biogas to biomethane. Biomass Bioenergy,2011,35:1633-1645.

[4] Sreenivasulu, B., Sreedhar, I., Suresh, P. & Raghavan, K. V. Development trends in porous adsorbents for carbon capture. Environ. Sci. Technol. 2015,49：12641–12661.

[5] Mohanty, P., Kull, L. & Landskron, K. Porous covalent electron-rich organonitridic frameworks as highly selective sorbents for methane and carbon dioxide. Nat Commun. 2011,401:2.

[6] J.D.V. Souza, E.S. Oliveira, A.R. Loiola, Zeolite A grown on fiberglass: A prominent CO_2 adsorbent for CO_2/ CH_4 separation. Colloids and Surfaces A. 2024,683:132952.

[7] N. Fu, B. Yang, Y. Wang, B. Shen, Y. Chen, W. Shao, Y. Yan, X. Wang, Z. Yang. Micromeso Hierarchical Porous Ultrathin Nitrogen-Doped Carbon Nanosheets with Rough Surfaces for Efficient Gas Adsorption and Separation. Energy Fuels 2022,36:13705-13712.

[8] J. Xiao, Y. Wang, T.C. Zhang, S. Yuan. N,S-containing polycondensate-derived porous carbon materials for superior CO_2 adsorption and supercapacitor. Applied Surf.Sci.2021,562:150128.

[9] O.T. Qazvini, R. Babarao, S.G. Telfer, Selective capture of carbon dioxide from hydrocarbons using a metal-organic framework. Nat.Commun.2021,197:2.

[10] G. Singh, I.Y. Kim, K.S. Lakhi, P. Srivastava, R. Naidu, A. Vinu, Single step synthesis of activated bio-carbons with a high surface area and their excellent CO_2 adsorption capacity, Carbon 2017,116:448–55.

[11] D. Wu, Y. Yang, J. Liu, Y. Zheng. Plasma-Modified N/O-Doped Porous Carbon for CO_2 Capture: An Experimental and Theoretical Study. Energy Fuels. 2020,34:6077-6084.

[12] Z. Jin, X. Jiang, Z. Dai, L. Xie, W. Wang, L. Shen, Continuous synthesis of nanodroplet-templated, N-doped microporous carbon spheres in microfluidic

system for CO2 capture. ACS Appl. Mater. Interfaces 2020, 12: 52571– 52580.
[13] Gu, S.; He, J.; Zhu, Y.; Wang, Z.; Chen, D.; Yu, G.; Pan, C.; Guan, J.; Tao, K. Facile carbonization of microporous organic polymers into hierarchically porous carbons targeted for effective CO_2 uptake at low pressures. ACS Appl. Mater.Interfaces 2016, 8: 18383– 18392.
[14] L.K.G. Bhatta, S. Subramanyam, M.D. Chengala, U.M. Bhatta, N. Pandit, K. Venkatesh, Investigation of CO_2 adsorption on carbon material derived from Mesua ferrea L. Seed cake, J. Environ. Chem. Eng. 2015, 3:2957–2965.
[15] M. Lillo-Rodenas, D. Cazorla-Amoros, A. Linares-Solano, Understanding chemical reactions between carbons and NaOH and KOH: an insight into the chemical activation mechanism, Carbon 2003,41: 267–275.
[16] L. Khezami, A. Chetouani, B. Taouk, R. Capart, Production and characterisation of activated carbon from wood components in powder: cellulose, lignin, xylan, Powder Technol. 2005,157: 48–56.
[17] M. Olivares-Marín, M.M. Maroto-Valer, Development of adsorbents for CO_2 capture from waste materials: a review, Greenh. Gases Sci. Technol. 2012,2: 20–35.
[18]] J. Ani, K. Akpomie, U. Okoro, L. Aneke, O. Onukwuli, O. Ujam, Potentials of activated carbon produced from biomass materials for sequestration of dyes, heavy metals, and crude oil components from aqueous environment, Appl. Water Sci. 2020,10:1–11.
[19] M. Iwanow, T. Gartner, V. Sieber, B. Konig, Activated carbon as catalyst support: precursors, preparation, modification and characterization, Beilstein J. Org. Chem. 2020,16:1188–1202.
[20] L.-Y. Hsu, H. Teng, Influence of different chemical reagents on the preparation of activated carbons from bituminous coal, Fuel Process. Technol. 2000,64:155–166.
[21] M. Plaza, A. Gonz´ alez, C. Pevida, J. Pis, F. Rubiera, Valorisation of spent coffee grounds as CO_2 adsorbents for postcombustion capture applications, Appl. Energy 201299:272–279.
[22] F. Rodríguez-Reinoso, Production and applications of activated carbons, Handbook of porous solids 2002,10:1766–1827.
[23] B. Sivakumar, C. Kannan, S. Karthikeyan, Preparation and characterization of activated carbon prepared from balsamodendron caudatum wood waste through various activation processes, Rasayan J. Chem. 2012,5: 321–327.
[24] T. Tay, S. Ucar, S. Karagoz, Preparation and characterization of activated carbon from waste biomass, J. Hazard. Mater. 2009,165: 481–485.
[25] R. Wang, P. Wang, X. Yan, J. Lang, C. Peng, Q. Xue, Promising porous carbon derived from celtuce leaves with outstanding supercapacitance and CO_2 capture performance, ACS Appl. Mater. Interfaces 2012,4: 5800–5806.
[26] A. Ahmadpour, D. Do, The preparation of active carbons from coal by chemical and physical activation, Carbon 1996,34: 471–479.
[27] J. Pavelec, J. Hulva, D. Halwidl, R. Bliem, et al, A multi-technique study of CO_2 adsorption on Fe_3O_4 magnetite, J. Chem. Phys. 2017,146: 014701.
[28] O. Gamba, J. Hulva, J. Pavelec, R. Bliem, M. Schmid, U. Diebold, G.S. Parkinson, Therole of surface defects in the adsorption of methanol on Fe_3O_4(001). Top. Catal. 2017,60: 420–430.
[29] T. Su, Z. Qin, G. Huang, H. Ji, Y. Jiang, J. Chen, Density functional theory study on the interaction of CO_2 with Fe_3O_4(111) surface. Appl. Surf. Sci. 2016,378: 270–276.
[30] A.H. Lahuri, A.A. Rahim, N. Nordin, R. Adnan, N.F. Jaafar. Y.H. Taufiq-Yap. Comparative studies on adsorption isotherm and kinetic for CO_2 capture using iron oxide impregnated activated carbon. Catalysis Today 2023,418:114111.
[31] O.T. Qazvini, R. Babarao, S.G. Telfer, Selective capture of carbon dioxide from hydrocarbons using a metal-organic framework, Nat. Commun. 2021,197:12.
[32] G. Singh, I.Y. Kim, K.S. Lakhi, P. Srivastava, R. Naidu, A. Vinu, Single step synthesis of activated bio-carbons with a high surface area and their excellent CO_2 adsorption capacity, Carbon 2017,116: 448–55.